THE JOURNAL OF PHYSICAL CHEMISTRY B

Article

pubs.acs.org/JPCB

The Effects of Chloride Binding on the Behavior of Cellulose-Derived Solutes in the Ionic Liquid 1-Butyl-3-methylimidazolium Chloride

Brooks D. Rabideau* and Ahmed E. Ismail

Aachener Verfahrenstechnik: Molecular Simulations and Transformations, Faculty of Mechanical Engineering, RWTH Aachen University, Schinkelstraße 2, 52062 Aachen, Germany

Supporting Information

ABSTRACT: The structure and diffusion of various linear and ringed solutes are examined in two different solvents, the ionic liquid 1-butyl-3-methylimidazolium chloride ([BMIM]Cl) and SPC/E water, using molecular dynamics (MD) simulations. The formation of distinctly ordered local solvent environments around these solutes is observed. Specifically, spatial distribution functions reveal significant ordering of the solvents around the solutes with chloride−hydroxyl group interactions largely dictating these arrangements. Further, a breakdown of the hydrogen bonds that develop between the solute and solvent is provided, showing a relationship between the presence of additional functional groups and the distribution of hydrogen bonds. The diffusivities of the solutes were determined in water at 298 K, 1 bar and [BMIM]Cl at 400 K, 1 bar. The results show that the solutes were approximately 10−100 times more diffusive in water than in [BMIM]Cl. Within [BMIM]Cl, diffusivity appears to decrease with increasing strength of the hydroxyl groups present. Additionally, the free energies of solvation of the solutes are determined with COSMO-RS, providing information about their tendencies in forming aggregates. These results are then compared with MD results in which aggregation is quantified through the use of a dispersion measure. Though all solutes remained relatively dispersed in each of the solvents, those with hydroxyl groups were seen to be the most highly dispersed in the solvent [BMIM]Cl. Further, the dynamic dispersal of a large solute aggregate into [BMIM]Cl was studied, finding that solutes with hydroxyl groups tend to form complexes with the chloride ions. If strong enough, these chlorides can actually bind multiple solutes together into long chains, inhibiting their dispersal in solvent. It is believed that the formation of these chloride−solute complexes is largely responsible for the decreased diffusivity and elevated dispersion seen in simulations with [BMIM]Cl.

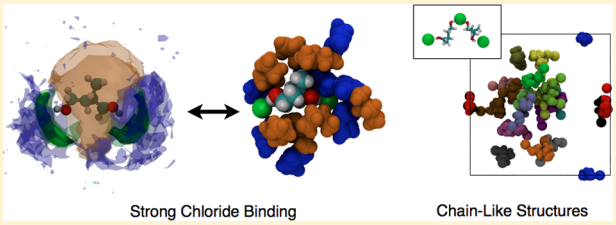

INTRODUCTION

The demand for a sustainable source of clean energy that does not interfere with the food chain has grown rapidly in recent years; creating "tailor-made" fuels from waste biomass offers one such solution. The challenge remains, however, to find energy-efficient and cost-effective processing and synthesis pathways with minimal environmental impact. One reaction mechanism currently under investigation is the conversion of cellulose-derived itaconic acid into 3-methyltetrahydrofuran (3-MTHF).[1] Ultimately, the success of any process will depend on its thermochemical properties, including the choice of solvents, the resulting dissolution behavior, the transport properties, and the presence of strong hydrogen bonds, which might inhibit desired reactions. Designing an optimal route for an industrial-scale biorefinery without prior knowledge of the properties of the various chemicals in these many possible pathways remains a difficult challenge. Current interest in the dissolution of cellulose by ionic liquids has led to the examination of the solvation behaviors of glucose[2,3] and cellulose[4−10] in different ionic liquids using both experimental and computational approaches.

Previous investigations relying on molecular simulations have examined the behaviors of different solutes with ionic liquid solvents. Studying the interactions of [MMIM]Cl with water, methanol, dimethyl ether, and propane, Hanke et al.[11] showed that hydrogen bonds between the solute and the anion dominate the solvation properties of solutes with hydroxyl groups. Moreover, it was reasoned that water and methanol could be thought of as forming water−chloride and methanol−chloride complexes which then interact with the imidazolium ion. A later study[12] examined the interactions of [DMIM]Cl and [DMIM]PF_6 with charged and uncharged models of benzene, and found that the electrostatic interactions between solute and solvent determine the local structure and the chemical potential. The interaction of [BMIM]PF_6 with the solutes methanol, water, acetonitrile, and *n*-hexane has also been examined:[13,14] by studying the radial distribution functions of atoms in these solutes with the anion, the polar imidazolium ring, and the nonpolar tail, a wide variety of behaviors between different solute types and different ionic liquid regions was found, illustrating the complex micro-structure formed within these solvents.

Received: February 7, 2012
Revised: July 5, 2012
Published: July 18, 2012

The hydration behavior of different solutes has also been examined. For example, a study focusing on the properties of water around the simple organic solutes methane, ethane, methanol, benzene, acetate, and methylammonium[15] concluded that, relative to the bulk, water structure is maintained around hydrophobic groups. Hernández-Cobos and Ortega-Blake studied an aqueous solution of methanol,[16] finding both hydration of the hydroxyl group as well as caging of the methyl group. Moreover, they also observed that, while the solute locally affects the structure of water, this effect is masked when averaged over the whole system.

In this study, we examine a number of intermediate chemicals in the itaconic acid to 3-MTHF pathway.[1] These six solutes, which include linear acids, linear diols, and ringed furans, are listed in Figure 1. In this paper, the properties of these solutes in the itaconic acid to 3-MTHF pathway and their interactions with the solvents water and the ionic liquid [BMIM]Cl (see Figure 2) are investigated. It was found that each of the solutes tend to interact with the solvent environments in their own unique way, which will be presented with both spatial and angular distribution functions. The diffusivities of these solutes were also calculated along with the developing hydrogen bonds between solute and solvent. Additionally, the tendency of each of the solutes to aggregate is examined, presenting both free energies of solvation as well as examining these tendencies via molecular dynamics. Finally, the dynamics of the dispersal of the solutes into solvent are examined; in doing so, we demonstrate that solutes containing multiple hydroxyl groups can form long "chain"-like structures, in which chloride ions connect adjacent solute molecules.

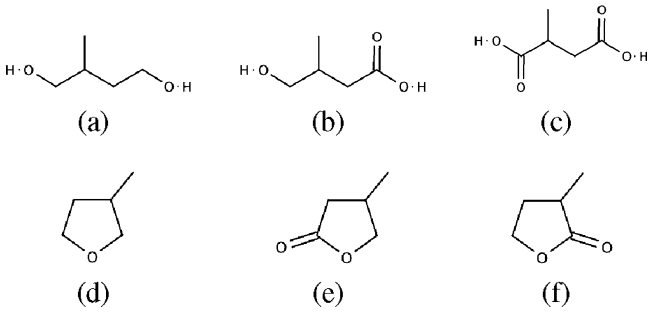

Figure 1. Chemicals in the itaconic acid to 3-MTHF pathway: (a) 2-methylbutane-1,4-diol (MBD), (b) 4-hydroxy-3-methylbutanoic acid (HMB), (c) 2-methylsuccinic acid (MSA), (d) 3-methyltetrahydrofuran (3-MTHF), (e) 3-methylbutyrolactone (3-MBL), and (f) 3-methyldihydrofuran-2(3*H*)-one (3-MDHF).

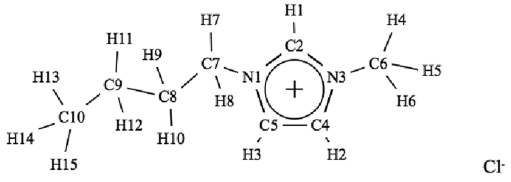

Figure 2. The structure of the ionic liquid 1-butyl-3-methylimidazolium chloride ([BMIM]Cl).

SIMULATION METHODS

Molecular dynamics simulations were performed using LAMMPS.[17] Solutes (see Figure 1) were modeled using the OPLS-AA force field,[18] while the SPC/E water model[19] was used in the aqueous simulations. Several different force fields exist for modeling imidazolium-based cations.[20−25] Unfortunately, many of these force fields were created before sufficient experimental data for these compounds were available. In the past few years, however, different studies have measured the densities of [BMIM]Cl.[26,27] Given that one of the focuses of the present study lies in the determination of the diffusivities of these solutes in [BMIM]Cl, a model that can accurately depict the density of the solvent would certainly be beneficial, as minor deviations in the density can lead to major deviations in the diffusivities as a result of changes in the free space available to the solute. Although this choice does not ensure accurate diffusivities, it does avoid this potential pitfall. With this in mind, [BMIM]Cl was modeled using the force field of Canongia Lopes and Padua,[20] as it appears to describe the temperature-dependent densities better than some of the other models examined.[22] Moreover, because the Canongia Lopes model is derived from the OPLS framework used to model the platform chemicals, it is not necessary to worry about parametrizing the cross-terms for interactions between [BMIM]Cl and the different solutes.

NEAT PATHWAY CHEMICALS: DENSITY AND SURFACE TENSION

To ensure that the OPLS-AA force field is able to accurately model the behaviors of the six pathway chemicals considered, the macroscopic behavior of each chemical was examined in its pure form. In this way, the performance of each model can be evaluated directly for self-consistency before applying these models in combination with the solvents. Others have examined similar chemicals using similar models[28] with good results; however, for completeness, each individual solute will be examined in this manner. To do this, two separate simulations were performed: one measuring the density and the other measuring the surface tension.

For the density simulations, approximately 400 molecules of each compound were placed in a periodic, cubic simulation box with side length of 40 Å. This was then simulated in an *NPT* ensemble at 298 K and 1 bar using a Nosé−Hoover thermo- and barostat,[29] with a damping constant of 100 fs for the thermostat and 1 ps for the barostat. A cutoff of 10 Å was used

Table 1. Calculated Densities and Surface Tensions of the Neat Platform Chemicals

name	ρ_{sim} (g/cm^3)	ρ_{pred} (g/cm^3)	γ_p (mN/m)	γ_{tail} (mN/m)	γ_{tot} (mN/m)	γ_{pred} (mN/m)
HMB	1.150	1.140[31]	39.3	8.2	47.5	44.1[31]
MBD	1.019	0.978[31]	34.8	7.3	42.1	36.6[31]
MSA	1.294	1.311[32]	70.0	10.7	80.7	53.2[31]
3-MBL	1.044	1.040[32]	24.5	7.6	32.1	29.3[31]
3-MDHF	1.061	1.040[32]	35.0	7.7	42.7	29.3[31]
3-MTHF	0.861	0.863[31]	14.4	7.7	22.1	25.4[31]

dx.doi.org/10.1021/jp305469p | *J. Phys. Chem. B* 2012, 116, 9732−9743

for both the dispersion and Coulombic interactions, and the particle−particle particle-mesh (PPPM) technique of Hockney and Eastwood[30] was used with an accuracy of 1 part in 10^4 to handle the long-range Coulombic forces. The densities of the pathway chemicals show a good overall agreement with the experimental values and are given in Table 1.

The surface tension simulations each use approximately 750 molecules, which were placed in the center of a 50 Å × 50 Å × 150 Å periodic simulation cell. This was then simulated in an *NVT* ensemble at 298 K using a Nosé−Hoover thermostat with a damping constant of 100 fs. As before, a cutoff of 10 Å was used for both the dispersion and Coulombic interactions and a PPPM grid with an accuracy of 10^{-4} was used to calculate the long-range electrostatic forces. The total surface tension can then be calculated as

$$\gamma = \gamma_p + \gamma_{tail} \tag{1}$$

where γ_p is the statistical mechanical definition of the surface tension[33]

$$\gamma_p = \frac{1}{2}\left[\langle p_{zz}\rangle - \frac{1}{2}(\langle p_{xx}\rangle + \langle p_{yy}\rangle)\right] \tag{2}$$

and γ_{tail} is a long-range tail correction[34,35]

$$\gamma_{tail} = \frac{\pi}{2}\int_{-\infty}^{\infty}\int_{-1}^{1}\int_{-r_c}^{\infty} r^3 U'(r) g(r)(1 - 3s^2) (\rho(z)\rho(z - sr) - (\rho_G(z))^2)\, dr\, ds\, dz \tag{3}$$

where $U'(r)$ is the pairwise potential, $g(r)$ is the radial distribution function, $\rho(z)$ is the observed interfacial profile, and $\rho_G(z)$ is the Gibbs dividing surface defined as

$$\rho_G(z) = r_c + \frac{\Delta\rho}{2}\,\mathrm{sgn}(z) \tag{4}$$

In this study, the density profile is fit to an error function, which has been shown to fit experimental data better than the typically assumed hyperbolic tangent profile.[36,37]

The total computed surface tension for each of the platform chemicals is compared with the experimentally reported and predicted values in Table 1. Relatively good agreement is seen for five of the six platform chemicals, with MSA being the clear exception. In reality, however, HMB and MSA are reported to be solids at standard temperature and pressure;[32] this could partially explain the deviation from the predicted properties in the simulations. A closer examination of the surface tension simulation of MSA showed that the molecules remain in an arrested state throughout the course of the simulations, with minimal translation and only minor molecular vibrations and slight rotations occurring. These cases aside, the agreement between the experimental and simulated densities and surface tensions provides confidence that these models reasonably depict the true behavior of these pathway chemicals. Furthermore, there is little indication that these models will have difficulties when they are extended to systems where little to no experimental data is available. These solute/solvent systems will be analyzed in the following sections.

DISTRIBUTION OF SOLVENT

To determine the solvent structure surrounding the different solvents, a 40 Å × 40 Å × 40 Å simulation cell of pure solvent was first equilibrated. In the case of water, this consisted of 2139 molecules and was simulated NPT at 300 K for 3 ns. In the case of [BMIM]Cl, this consisted of 238 ion pairs which were simulated in an *NPT* ensemble and slowly heated to 500 K over the course of 1 ns, simulated at 500 K for another nanosecond, and then returned to 400 K over another nanosecond. Finally, it was equilibrated at 400 K for another 3 ns. Twelve different simulations were then devised: five molecules of each of the six solutes were randomly placed into equilibrated samples of either water or [BMIM]Cl. Solvent molecules that overlapped with the solute molecules were removed; for [BMIM]Cl, this meant removing cations and ions in a 1:1 ratio to maintain a charge neutral system. The resulting systems were then run in an *NPT* ensemble for 3 ns and continued for another 50 ns in the case of water and 90 ns in the case of [BMIM]Cl in an *NVT* ensemble. In all cases, the cutoff length, PPPM grid, and damping constants were the same as above. In the next few sections, it will be shown that this 50−90 ns should provide an adequate sampling of the local solvent environment around each solute.

It has been shown that ionic liquids affect the local environments around solutes depending upon the relative polarity and associative behaviors of the solutes as well as the structure of the ionic liquid.[13,14] This has been demonstrated through the use of radial distribution functions between the various atomic species of the solute with the atomic species of the solvent, such as the alkane tail, the polar "head" group, or the anion. This analysis, however, is severely limited in that it only gives information about the relative radial distance between one species and another. Determining the precise three-dimensional location of one atom with respect to another atom, in essence a spatial distribution function, can be used to gain clearer insight into the ordering around molecules. Moreover, this view allows much more information to be obtained pertaining to the different solvent domains present around these solutes.

Here, the local environments are reconstructed around each of the solutes. Since the solutes' positions and orientations change throughout the course of the simulation, this change must be accounted for in the determination of the solvent orientation relative to the solute instead of just simply relative to the simulation box as is given. To do this, three atoms are defined in each solute that will define the solute's coordinate system at each time step and determine the positions of the solvent relative to this. In the case of the linear solutes, the hydroxyl oxygen atoms and the methyl carbon atom were used to define its orientation; in the case of the ringed compounds, the furan oxygen atom was selected along with two adjacent carbon atoms. The specific locations of these atoms are given in the Supporting Information. In applying this method, solvent atoms were binned into appropriate cubic cells according to their position relative to the orientation of the solute molecule.

It should also be noted that the atoms within each solute molecule also undergo relative motion throughout the course of the simulation. In this case, one cannot completely recover the precise locations of each of the constituent atoms from one time step to the next and, hence, the solvent orientation could be slightly off. One could expect, however, that this motion has some sort of mean positional arrangement and through averaging over a suitable amount of time steps that the mean solvent position around the mean conformation of the solute will be obtained. In the case of the ringed solutes, this movement is quite small due to the rigidity of the furan ring, and one would expect a very good reconstruction of the atomic positions at each time step.

dx.doi.org/10.1021/jp305469p | J. Phys. Chem. B 2012, 116, 9732−9743

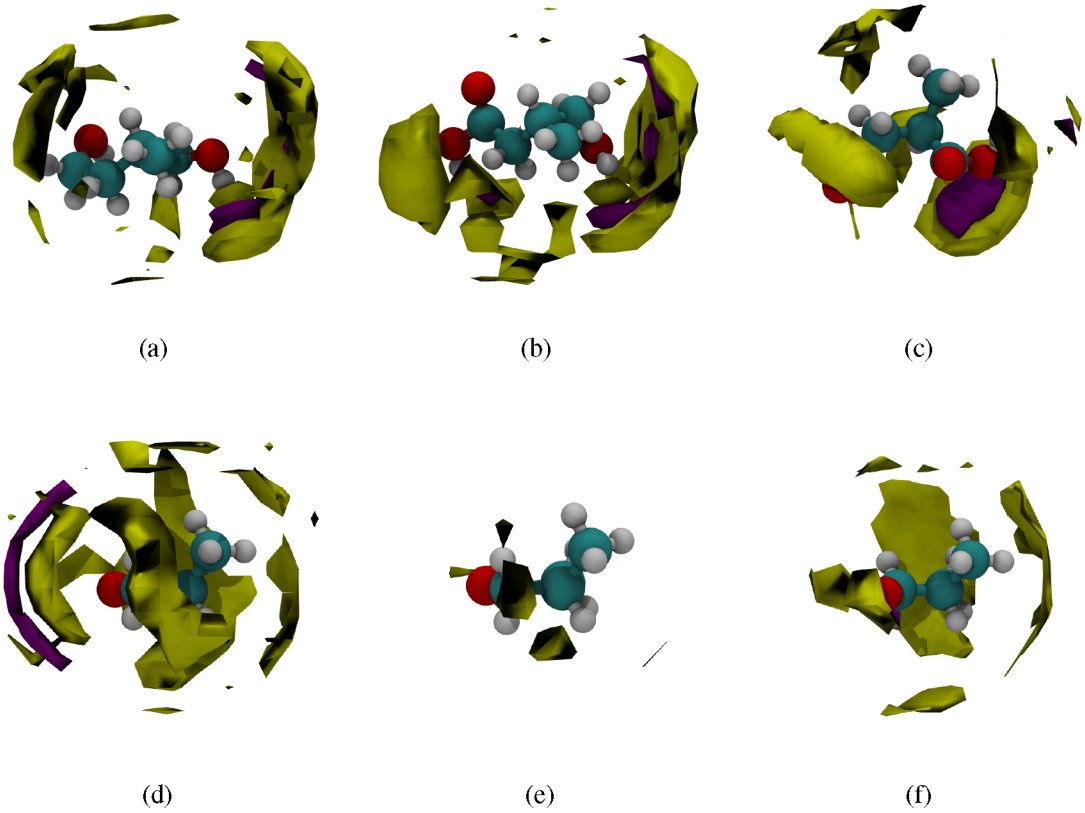

Figure 3. Three-dimensional probability distributions of water solvent around the solutes (a) MBD, (b) HMB, (c) MSA, (d) 3-MTHF, (e) 3-MBL, and (f) 3-MDHF. Colors indicate enhanced densities of water oxygens (purple) and water hydrogens (yellow). Solid purple regions are 2 times the normal density, and solid yellow regions indicate 1.25 times the normal density.

The spatial distribution functions of the water solvent surrounding each of the six different solutes are shown in Figure 3. In this figure, the purple regions indicate an increased density of the water oxygen atoms relative to the bulk, while the yellow regions indicate an increased water hydrogen density relative to the bulk. The distributions for lower densities are given in the Supporting Information and show spherical shells of water oxygen atoms surrounding each of the solute molecules. There appears to be a slight preference for water hydrogen to reside near the hydroxyl groups of the linear solutes and the oxygen groups of the ringed compounds.

A special orientational dependency is shown for 3-MTHF in Figure 3, in which there exists a small crescent-shaped region of increased water hydrogens directly in front of the lone oxygen atom. This is then followed at a slightly further radial distance by another crescent-shaped region of increased water oxygen atoms directly in front of the oxygen atom. This indicates the preferential orientation sought by the water molecules in hydrogen bonding with the furan oxygen. The water hydrogen atom is the closest to the furan atom, while the water oxygen atom is farthest away from the furan oxygen atom.

The spatial distribution functions of the [BMIM]Cl around each of the solute molecules is displayed in Figure 4. The three different colors in the figures indicate different solvent domains: green and blue indicate increased density regions of the chloride ion and the [BMIM] cation (C_2), respectively. Figures providing the orientational dependence of the [BMIM] tail group are given in the Supporting Information, though generally these regions occupy the voids surrounding the molecules of Figure 4. Clearly, the chloride anions like to reside near the hydroxyl groups of the linear solutes and form cusps around each of the groups at both ends of the molecule. The ringed solutes show a slightly different behavior with regard to the anion. While the chloride anions show only a slight preference in their ordering around 3-MTHF, around 3-MBL and 3-MDHF, there exists an enhanced density region that takes the form of a thin ring whose radius is positioned perpendicular to the plane of the furan ring. Furthermore, these rings are more weighted toward the sides opposite the carbonyl group, with the two cases being near-mirror images of each other, as would be expected due to the near-symmetry of the molecules.

Examining the different plots in Figure 4, one begins to see the segregation of the head and tail domains of [BMIM] relative to the solutes. This is most clearly seen in Figure 4a and in Figure 4f. In the first case, the cations are weighted toward the ends of the linear molecule as are the chloride ions. This leaves the tail domains in the center, represented by the void space around the molecule, and as such they can reside near the nonpolar backbone of this molecule. In Figure 4f, the [BMIM] cations prefer to position themselves in front of the oxygen atoms and to a lesser extent near the thin, chloride-rich ring, while the tails associate with the remainder of the molecule.

These figures indicate that the presence of different solvent domains around each solute might be seen more clearly from the use of an angular distribution function $g(\theta)$, in which θ is the azimuthal angle of a spherical coordinate system located at the center of mass of the solute:

$$g(\theta) = \frac{V^N}{Z} \int_V \exp\left[\frac{-U(\mathbf{r}_1, \mathbf{r}_2)}{k_B T}\right] r_1^2 \sin\phi \, dr_1 \, d\phi \, d\mathbf{r}_2 \quad (5)$$

dx.doi.org/10.1021/jp305469p | J. Phys. Chem. B 2012, 116, 9732−9743

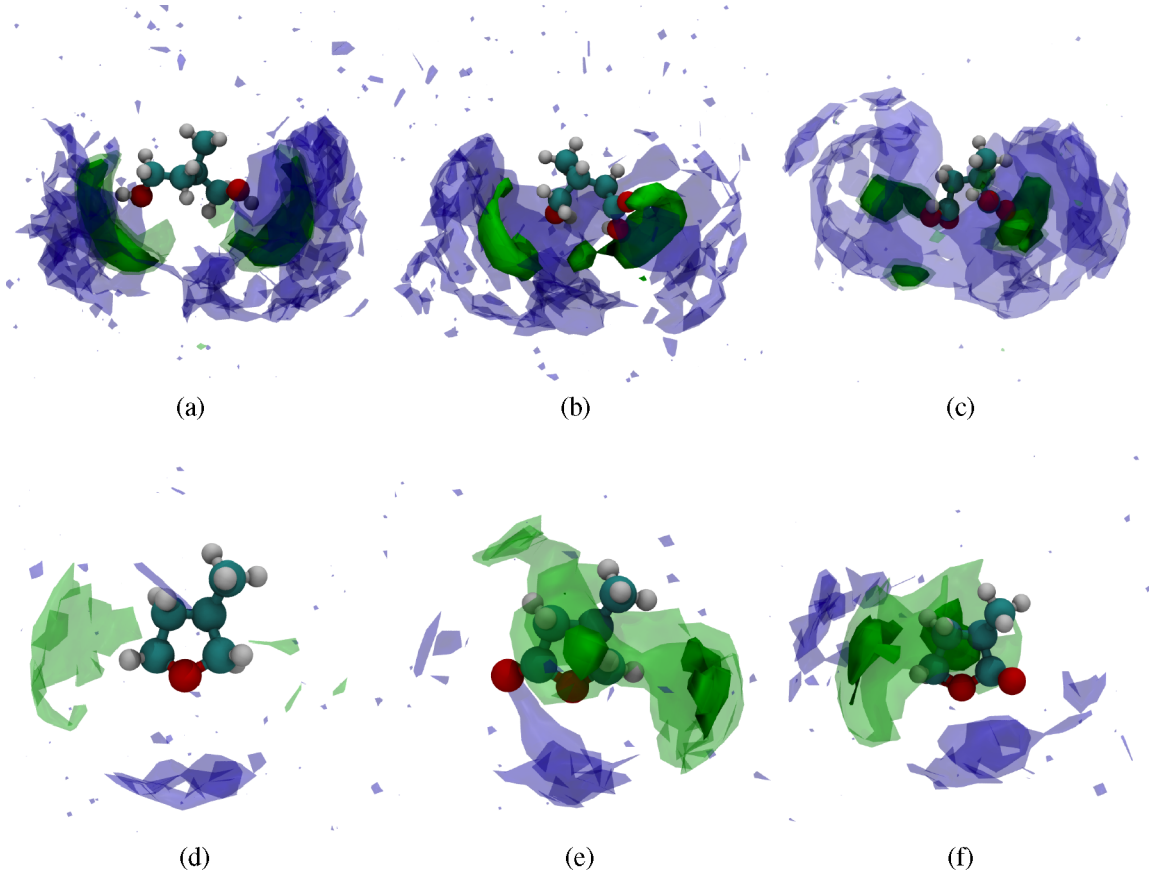

Figure 4. Three-dimensional probability distributions of [BMIM]Cl solvent around the solutes (a) MBD, (b) HMB, (c) MSA, (d) 3-MTHF, (e) 3-MBL, and (f) 3-MDHF. Colors indicate enhanced densities of chloride ions (green) and [BMIM]'s C_2 atom (blue). Relative to the bulk, the isosurfaces are as follows: solid green, 4×; transparent green, 2×; transparent blue, 1.5×.

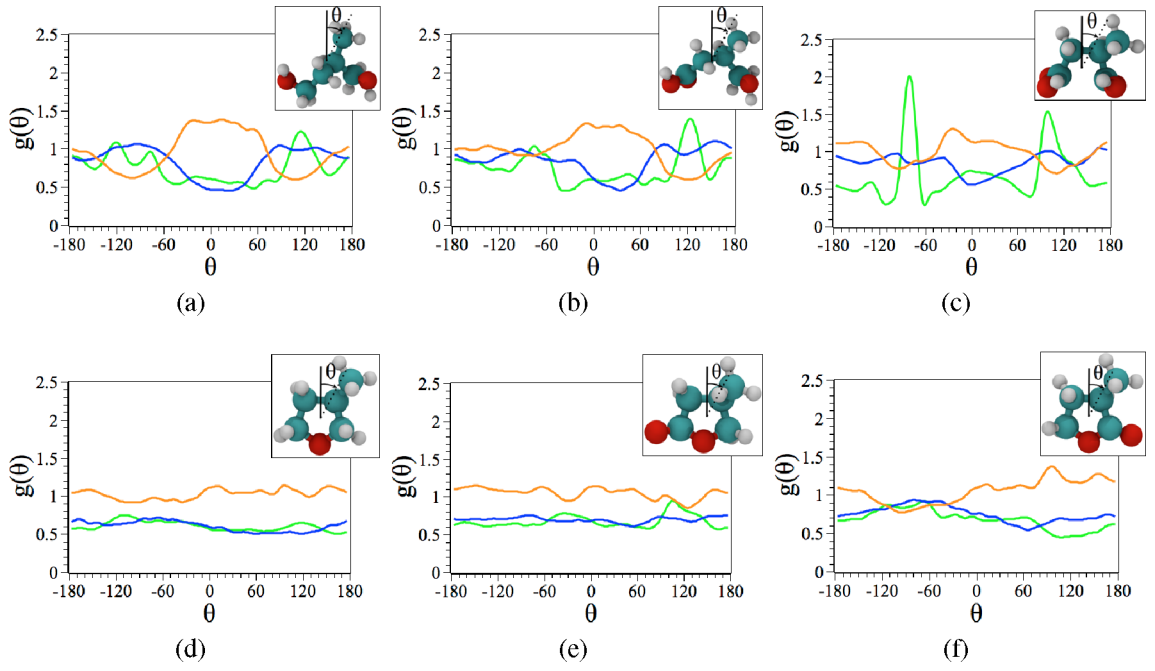

Figure 5. $g(\theta)$ for the solutes (a) MBD, (b) HMB, (c) MSA, (d) 3-MTHF, (e) 3-MBL, and (f) 3-MDHF for the Cl anion (green), the [BMIM] cation (blue), and the [BMIM] tail (orange).

where Z is the canonical partition function. This function can be constructed by placing the specified solvent atoms into the corresponding angular bins around each solute molecule, including all of the atoms which exist within a cutoff radius R_c (in this case 8 Å) from the center of mass of the solute. This function can then be normalized, in much the same manner as

dx.doi.org/10.1021/jp305469p | J. Phys. Chem. B 2012, 116, 9732−9743

in the calculation of a radial distribution function, by dividing by the volume of the bin and the expected bulk density. The angular distribution function $g(\theta)$ is given for each of the solutes in Figure 5.

Here, the angular dependence of the solvent domains around each solute has been quantified. The strongest indication of this is shown for MSA in Figure 5c. Near the two end carboxyl groups, at approximately −90 and +90°, there is a drastic increase in the presence of chloride and the [BMIM] cation in this area relative to the bulk. Consequently, there is a decreased presence of [BMIM] tail groups here. Instead, the tails prefer to reside near the nonpolar backbone of the molecule located from approximately −45 to +45°.

A snapshot of MBD showing only the contacting solvent molecules is shown in Figure 6. Here, the coloring scheme is

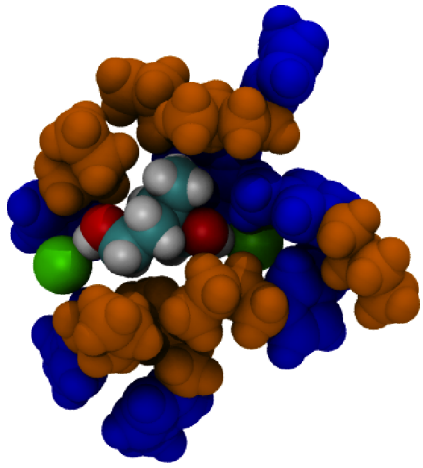

Figure 6. A snapshot of MBD showing only the solvent molecules in contact with the solvent. Green indicates chloride, blue indicates the [BMIM] cation, and orange indicates the [BMIM] tail.

the same as in Figure 4 and the orientation of solvent molecules around MBD is representative of all of the snapshots observed. One item that is captured in this snapshot is the binding of the chloride ions to the hydroxyl groups. For each solute possessing hydroxyl groups, similar behavior was observed. For the first few nanoseconds of the simulation, as the [BMIM]Cl solvent rearranges, different chloride ions bind and free themselves from the hydroxyl groups. After this initial ∼5 ns period, however, a given chloride ion will bind with each hydroxyl group and remain "bound" for the remaining 40 ns of the simulation. This is in agreement with previous findings[11] which suggested that the chloride ions first bind with the hydroxyl groups and this entire complex then interacts with the cation. The results of the spatial distribution functions in Figure 4 support this finding, showing a strong presence of chloride ions near the hydroxyl groups, followed closely thereafter by the [BMIM] cation. The [BMIM] tail then is left to interact with any remaining and exposed, nonpolar regions of the molecule.

HYDROGEN BONDING

A set of geometric criteria[38−43] was used to determine the presence of hydrogen bonds between the water solvent and the single solute of each simulation. Specifically, the requirements hold that the distance between the hydrogen to the accepting oxygen must be less than 2.45 Å, the distance between the two oxygen atoms must be less than 3.5 Å and the oxygen acceptor−oxygen donor−hydrogen angle must be less than 30° for the interaction to be considered as a hydrogen bond. This set of criteria is outlined in Figure 7.

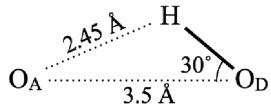

Figure 7. Geometric criteria employed in this study for the determination of H-bonds.

This set of criteria was applied to snapshots taken at 20 ps intervals for the simulations described above. The average number of hydrogen bonds for each of the solutes in SPC/E water is displayed in Figure 8. As expected for the linear solutes

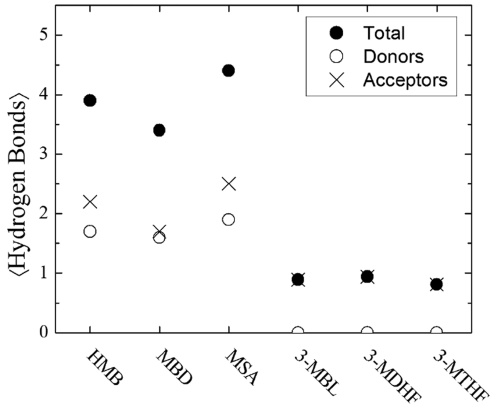

Figure 8. The average number of hydrogen bonds formed between each solute and the water solvent.

(HMB, MBD, and MSA), the average number of hydrogen bonds increases with the number of oxygen atoms present in the solute and ranges from about 3.5 to almost 5 total hydrogen bonds at any one time. The number of hydrogen bonds in the ringed solutes, conversely, shows very little dependence on the number of oxygen atoms present in the solute. The pronounced difference in behavior between the linear and ringed solutes can be attributed to the linear solutes containing hydroxyl groups that can serve as both hydrogen donors as well as acceptors, while the ringed solutes can only receive hydrogen bonds from the surrounding solvent. The figure also shows that there is a large discrepancy between the number of hydrogen bonds accepted by the ringed solutes versus the linear solutes, with the linear solutes accepting nearly twice as many bonds as the ringed solutes.

A more detailed view of this hydrogen bonding, given on a per-atom basis, is shown in Figure 9. Here, the presence of additional functional groups to each solute can be seen. For example, the addition of a carbonyl group next to a hydroxyl group tends to reduce the hydroxyl oxygen acceptance by roughly half, and increase the hydroxyl-hydrogen donation slightly. The carbonyl itself draws ∼3/4 of a hydrogen bond from the surrounding solvent. Alternatively, the addition of a carbonyl group next to a furan oxygen still draws ∼3/4 of a hydrogen bond; however, this leads to an overall reduction to ∼1/4 of a hydrogen bond in the case of the furan oxygen.

For a more detailed view of the hydrogen bonds being formed and their associated lifetimes, the previous simulations were extended another nanosecond, this time with a fine

dx.doi.org/10.1021/jp305469p | J. Phys. Chem. B 2012, 116, 9732−9743

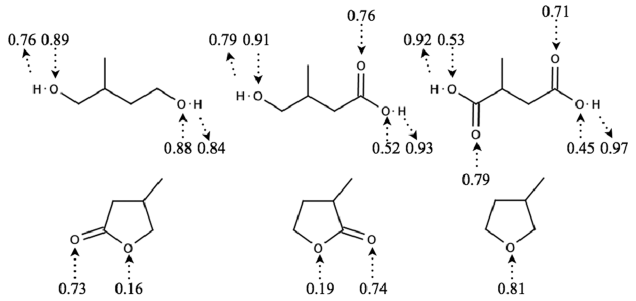

Figure 9. Detailed breakdown of the average number of hydrogen bonds being donated to each atom and accepted by each atom.

sampling interval of 0.5 ps. Each time step was evaluated and the hydrogen bonds determined via the geometric criteria. The hydrogen bonds were followed for each time step, and those present in successive timesteps were deemed not to have broken. In water, all six solutes exhibited a roughly exponential decay in the histogram of lifetime values. The breakdown of the average hydrogen lifetime for each solute by functional group is given in Table 2.

Average hydrogen bond lifetimes encompass several orders of magnitude: the carboxylic hydrogen donates the longest-lived hydrogen bond at approximately 32 ps, while the furan oxygen next to a carbonyl is the shortest lived at 0.090 ps. Surprisingly, the lone furan oxygen is significantly longer lived when there is no carbonyl oxygen next to it, a fact which might contribute to the structural ordering seen near the furan oxygen for 3-MTHF in Figure 3.

DIFFUSIVITY

To determine the diffusivities of each of the compounds in each of the solvents, a new series of simulations were carried out. In each simulation, five molecules, all of the same molecule type, were placed randomly in a cubic simulation cell of side length 40 Å. This was then run in an *NPT* ensemble for a period of 3 ns (at their respective temperatures and pressures) followed by production runs in the *NVT* ensemble for upward of 100 ns. Previous works examining the role of the thermostat on diffusion results showed little differences[44] between the use of an *NVE* ensemble and the use of a weakly coupled thermostat.

Details for each of the separate simulations can be found in the Supporting Information. Among other things, it was ensured that each solute traveled, on average, 3 times the respective molecular diameter of the solute. This criterion was essentially fulfilled for every solute−solvent pair other than MSA in [BMIM]Cl, which showed the slowest diffusive motion overall. In this case, solutes traveled an average of only 2.3 molecular diameters, despite almost 90 ns of simulation. Additionally, log−log plots were analyzed to determine the regions in which the solutes exhibit normal diffusion:

$$D_{\text{self}} = \frac{1}{6}\lim_{t\to\infty}\frac{\mathrm{d}}{\mathrm{d}t}\langle |r_i(t) - r_i(0)|^2\rangle \tag{6}$$

where D is the diffusivity constant and the quantity in brackets is the mean square displacement of an individual molecule. Each of the five solutes of each simulation was analyzed independently, and the mean and errors of the resulting diffusivities were calculated. Only the solutes showing a sustained period of normal diffusion were included in the final averaging, which can be found in Figure 10. All of the details of each individual solute, including region of fit, log−log slope, and calculated diffusivity, can be found in the Supporting Information.

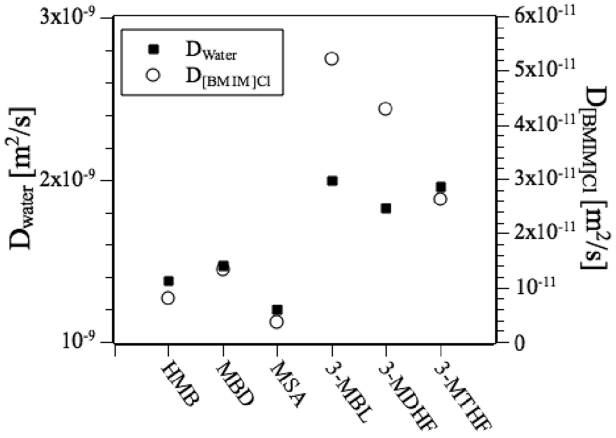

Figure 10. Diffusivities of the different compounds in water and [BMIM]Cl.

The results show that the solutes diffuse nearly 10−100 times faster in SPC/E water than in [BMIM]Cl, despite the latter simulations being carried out at an elevated temperature of 400 K. Interestingly, the ringed compounds 3-MBL, 3-MDHF, and 3-MTHF, which are largely nonpolar, diffuse almost twice as fast in the case of water and nearly 4 times as fast in [BMIM]Cl as the linear compounds HMB, MBD, and MSA. Further, among the linear compounds, the diffusivities tend to decrease with relative strength of the hydroxyl groups present. For example, MSA, with two carboxyl groups, has a lower diffusivity than HMB, which has one carboxyl and one hydroxyl group; in turn, HMB has a lower diffusivity than MBD, which has only two hydroxyl groups. Interestingly, these three linear compounds were shown to have strong associations with the

Table 2. Breakdown of Hydrogen Bond Lifetimes (Given in ps) by Functional Group[a]

functional group	HMB	MBD	MSA	3-MBL	3-MDHF	3-MTHF	average
carboxylic H	30		33, 32				32
alcohol H	1.4	1.5, 1.6					1.5
alcohol O	1.3	1.5, 1.6					1.4
furan O						0.76	0.76
carboxylic O	0.44		0.39, 0.43				0.42
carboxylic =O	0.43		0.41, 0.43				0.42
furan =O				0.31	0.41		0.34
furan O (next to =O)				0.086	0.094		0.090

[a]Multiple entries indicate multiple functional groups per molecule and are reported separately for comparison.

dx.doi.org/10.1021/jp305469p | J. Phys. Chem. B 2012, 116, 9732−9743

Table 3. Free Energies of Solvation $\Delta_{solv}G$ (Given in kcal/mol) for the Six Different Solutes[a]

	298 K			400 K		
solute	ΔG_{neat}	ΔG_{H_2O}	ΔG	ΔG_{neat}	ΔG_{IL}	ΔG
HMB	−10.3	−9.75	0.564	−7.42	−9.92	−2.50
MBD	−9.78	−8.94	0.837	−6.98	−7.88	−0.906
MSA	−11.3	−11.4	−0.145	−8.52	−12.4	−3.91
3-MBL	−8.19	−7.57	0.628	−7.16	−6.75	0.408
3-MDHF	−8.19	−7.52	0.682	−7.17	−6.76	0.410
3-MTHF	−5.05	−3.51	1.54	−4.17	−3.41	0.758

[a]The thermal energy at 298 K is k_BT = 0.592 kcal/mol and k_BT = 0.795 kcal/mol at 400 K.

chloride ions of [BMIM]Cl, as seen from the spatial distribution functions. The stronger association with chloride ions would effectively increase the mass of these complexes, and thus, a lower diffusivity would be expected. Moreover, one might expect that these negatively charged complexes would have to overcome electrostatic charge barriers during their diffusion through the ionic medium. In the next sections, further consequences of these chloride−hydroxyl interactions will be explored.

FREE ENERGY OF SOLVATION

Ultimately, the transport and separation of solute from solvent will depend heavily upon the underlying tendencies of each solute. For example, a solute tending to assemble into larger clusters within the solvent will generally have slower diffusion rates, something that could strongly impact the design of an adequate separation process. Thus, the tendency of each solute to aggregate with other solutes or remain dispersed in the solvent medium is of tremendous interest in the preliminary process design.

A quantitative measurement of this tendency to associate is the free energy of solvation, $\Delta_{solv}G$, which can be determined from the individual values from both the neat and solvated states. It is possible to obtain these values through molecular dynamics simulations however at a large computational cost.[45−51] Moreover, special techniques must be applied when dealing with certain solutes to ensure an adequate sampling of phase space. Previously, it was shown that carboxylic acids, not unlike the ones in this study, should receive this special treatment to avoid this sampling pitfall.[52]

Arguably, a more direct calculation of the free energies of solvation could be obtained through the use of continuum solvation models. Not only have many of these models been parametrized for industrial application, they require only a fraction of the computational cost of MD methods and have proven to be quite reliable in blind studies.[53] Since our overall interest is in practical values, we compute the energies of solvation using COSMOtherm.[54,55] Relevant solute and solvent conformers were also taken into consideration, having been identified with the aid of COSMOconf. The free energies of solvation for each solute in its neat form and in water at 298 K and in its neat form and in [BMIM]Cl are given in Table 3.

Overall, the majority of the free energy differences between neat and solvent cases are comparable with the amount of thermal energy present in each system (k_BT = 0.592 kcal/mol at 298 K and k_BT = 0.795 kcal/mol at 400 K). In the following section, very little aggregation of the solutes is seen in either of the solvents, most likely a result of this proximity with thermal energy. The main exception to this is 3-MTHF in water, which has the largest free energy difference, most likely a result of its nonpolar character. Conversely, the linear solutes MSA, HMB, and to a lesser extent MBD have a strong urging to associate with the solvent [BMIM]Cl.

AGGREGATION

In the previous section, free energies of solvation were calculated for each of the solutes using a continuum solvation method. In this section, these thermodynamic values will be related with the underlying solute behavior as seen from molecular dynamics simulations. Specifically, the degree of aggregation of solutes within solvent is quantified with a dispersion measure that was introduced by Clark and Evans.[56] The dispersion measure is defined as

$$\langle R \rangle = \frac{\langle R_A \rangle}{\langle R_E \rangle} \tag{7}$$

where $\langle R_A \rangle$ is the mean nearest neighbor distance and $\langle R_E \rangle$ is the expected mean of the nearest neighbor distance for a randomly distributed system.

The dispersion measure relates the degree of aggregation relative to a randomly dispersed system. A value of $\langle R \rangle$ equal to unity indicates a system that is randomly distributed, while a completely clustered group of solutes would correspond to a value of $\langle R \rangle$ equal to zero. For real solutes, and not point particles, this measure would actually be slightly above zero owing to the volume exclusion. When $\langle R \rangle$ is greater than unity, this indicates a certain amount of uniformity that is present in the system.

This series of simulations was conducted by placing 20 identical solute molecules in random locations within a cubic simulation box with a side length of 40 Å. This box was already filled with pre-equilibrated solvent molecules, so some solvent molecules had to be removed as the new solute molecules were added. Each solute/solvent system was then simulated in the *NPT* ensemble for 3 ns, followed by production runs in the *NVT* ensemble. Production runs for the [BMIM]Cl and the water simulations were approximately 120 ns and approximately 50 ns, respectively. The longer simulation time for [BMIM]Cl ensured that the solutes would have enough time to diffuse throughout the simulation box and ensure adequate spatial sampling. Extrapolating the mean squared displacements from the diffusivity simulations for [BMIM]Cl (given in the Supporting Information) indicates that this 120 ns of simulation time should allow the solutes to travel an average of over 4 nearest neighbor distances $\langle R_E \rangle$ and in the case of MSA, the slowest solute, at least 2 nearest neighbor distances. The 50 ns simulations for water should provide a much more elevated level of sampling with each solute expected to travel over 40 nearest neighbor distances. The water simulations were conducted at 298 K and 1 bar, and the [BMIM]Cl simulations

dx.doi.org/10.1021/jp305469p | J. Phys. Chem. B 2012, 116, 9732−9743

were conducted at 400 K and 1 bar. The dispersion measure of eq 7 was calculated for each of the cases and the results given in Figure 11.

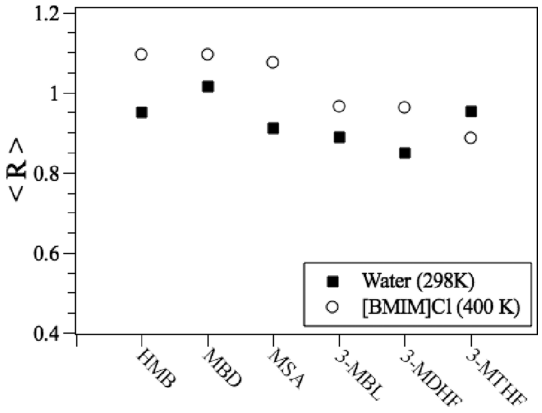

Figure 11. The time-averaged dispersion measure $\langle R \rangle$ in eq 7 for all six solutes.

The values of $\langle R_E \rangle$ can be determined from theoretical considerations, however, in this study were determined via simulation. Lower limits of the dispersion measure were determined for the corresponding neat liquids, yielding values of approximately 0.35 for each of the solutes. In all cases, both in the water and the [BMIM]Cl solvents, the solutes remain largely dispersed. 3-MDHF in water, with $\langle R \rangle \sim 0.85$, showed the greatest tendency to aggregate. This aggregation however is generally short-lived, and dominated by the interplay between formation and breakup. Overall, the solutes are more highly dispersed in [BMIM]Cl when compared to water. One possible explanation for this is the association of chloride ions with the solutes themselves and the ensuing mutual repulsion of these negatively charged complexes. This seems especially true for the linear solutes HMB, MBD, and MSA, whose hydroxyl groups tend to form strong associations with chloride, as seen from the spatial distribution functions. A plot of the dispersion measure $\langle R \rangle$ versus the free energy of solvation $\Delta_{solv}G$ can be found in Figure 12. As expected, this measure is inversely proportional to the free energy of solvation.

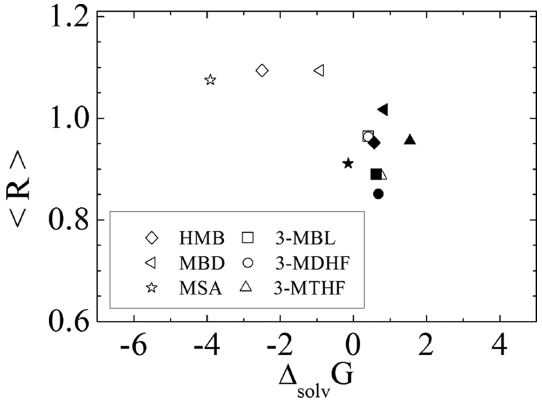

Figure 12. The time-averaged dispersion measure $\langle R \rangle$ versus $\Delta_{solv}G$. Solid symbols indicate simulations with water at 298 K, and empty symbols indicate simulations with [BMIM]Cl at 400 K.

DYNAMIC DISPERSAL OF SOLUTE

To study the dynamic behavior of solute dispersal throughout the solvent [BMIM]Cl, a new series of simulations were performed. This time, the solutes were no longer placed in random locations within the simulation box but rather placed together as a spherical droplet at the center of the simulation box. All other aspects of the simulation were conducted just as the aggregation simulations in the previous section.

The evolution of the dispersion measure can be found in the Supporting Information. As expected, the results show an upward drift of the dispersion measure for each of the solutes, toward the long-time values observed in Figure 11. An examination of the underlying structure of the solutes during this time, however, revealed some surprising results.

The dispersion measure indicates how aggregated or dispersed a system is relative to a randomly dispersed system, although it does not reveal much information about the underlying structure. For instance, the dispersion measure makes little distinction between a phase-separated solute droplet and a percolated chain network. A much better indicator of this is the average number of nearest neighbors. To calculate this value, a distance criterion must be established, which will indicate that two solute molecules are neighbors. Here, the distance that corresponded to the longest distance associated with the initial peak in the center-of-mass to center-of-mass radial distribution functions was determined from simulations of the corresponding neat liquids. Employing this as the neighboring criterion allowed for the calculation of the average number of neighbors, and the results are given in Figure 13.

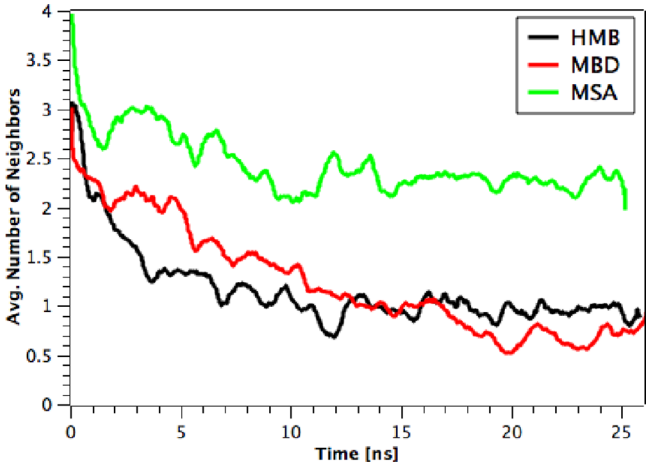

Figure 13. The average number of neighbors calculated during the dissolution simulation for the linear solutes.

The figure shows a sustained decrease in the average number of neighbors for all of the linear solutes over the course of the 25 ns. MSA, however, has a slower decline relative to HMB and MBD and once it reaches a value of approximately 2.5 neighbors appears resistant to any further reduction.

A look at the underlying structures in Figure 14 gives insight into why this might be. Figure 14 shows the resulting structures of the MBD and MSA simulations at the end of the 25 ns. In addition to the solutes, all of the chloride ions deemed to be in contact with the solutes are also shown. "Contact" was defined as the longest distance associated with the initial peak in the Cl to hydroxyl hydrogen radial distribution function. Interestingly,

dx.doi.org/10.1021/jp305469p | J. Phys. Chem. B 2012, 116, 9732–9743

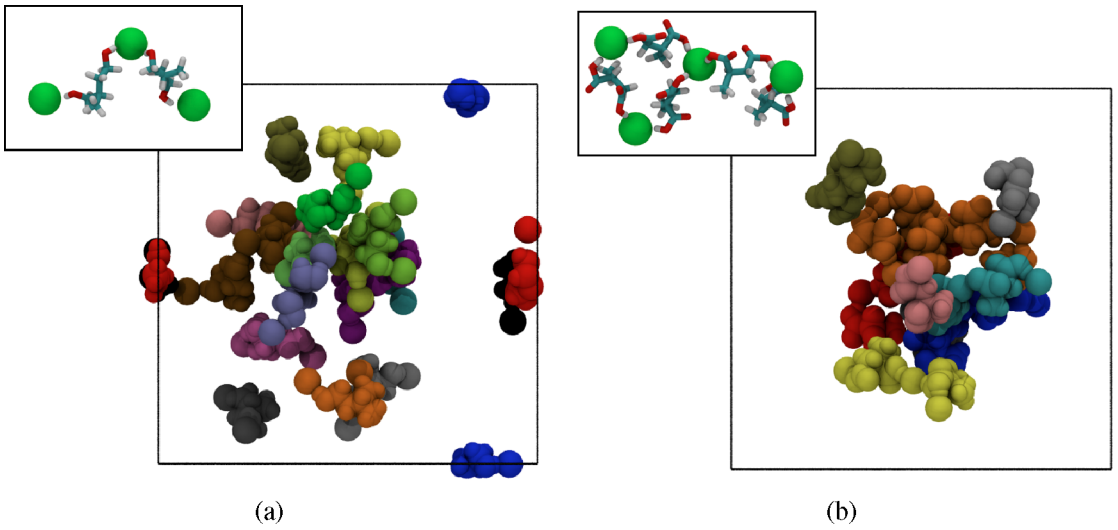

Figure 14. The arrangement of an initially spherical drop of solute of (a) MBD after 25 ns and (b) MSA after 25 ns. Colors indicate individual chloride-bound clusters. The remaining solvent has been suppressed from each figure. Insets show the largest cluster present in each system.

the results showed a number of solute−chloride complexes, formed through the association of chloride with the hydroxyl groups of each solute. Each complex was colored separately in Figure 14, which shows significantly fewer yet larger complexes in the case of MSA when compared with MBD. The largest solute−chloride complex of each subfigure can be found in the insets. Here, it becomes clear that MSA forms long, chain-like structures formed by the connection of the strong carboxylate ends together via connecting chlorides. Although hydroxyl ends are still present in MBD, they tend to have a weaker interaction, allowing unbound chlorides to break these chain networks apart. From these figures, it appears that MSA has a significantly reduced dispersal in [BMIM]Cl owing to this strong connection of multiple solute ends together via bound chlorides.

Another perspective on this clustering can be obtained by analyzing the distribution of cluster sizes observed during the simulations (see Figure 15). Here, cluster size refers to the total number of solute molecules and chloride ions that comprise one interconnected complex. Unlike the histograms of HMB and MBD (not shown), which show an exponential decay in the probability of finding larger cluster sizes, the histogram of MSA shows an equal probability of clusters, independent of cluster size, for clusters of roughly 10 molecules or more.

To determine whether or not differences in the dispersion parameters of alcohol OH groups and carboxylate OH groups were solely responsible for the observed binding effect, the dispersion parameters of both the oxygen and hydrogen composing each hydroxyl group were switched between MBD and MSA and the simulations repeated. Electrostatic charges were not exchanged. It was found that the addition of carboxylate OH parameters to MBD was not sufficient in causing this binding effect to occur, while the addition of alcohol OH parameters to MSA did reduce but did not fully prevent this binding from taking place. Further details of these results can be found in the Supporting Information.

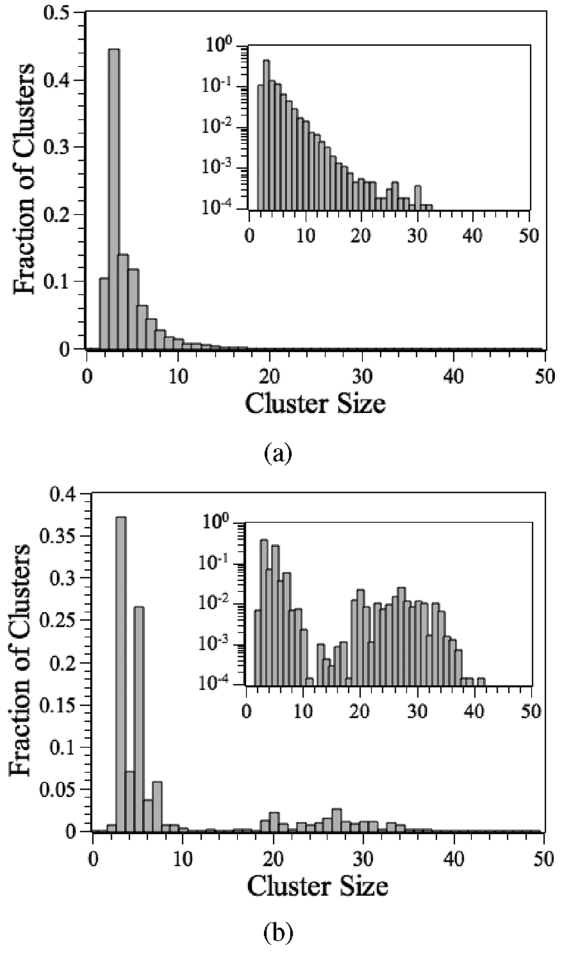

Figure 15. The distribution of cluster sizes during the dissolution of (a) 20 HMB molecules and (b) 20 MSA molecules in [BMIM]Cl. Cluster sizes include bound chlorides. Insets are shown in semilog format.

CONCLUSIONS

The structure and diffusion of various linear and ringed compounds along a potential cellulose to biofuel pathway were examined in the solvents [BMIM]Cl and water. Each compound showed a remarkably different local solvent structure. It was observed that water tends to orient around hydroxyl and furan functional groups, while chloride−hydroxyl group interactions tend to dominate solvent ordering in

dx.doi.org/10.1021/jp305469p | J. Phys. Chem. B 2012, 116, 9732−9743

[BMIM]Cl, with [BMIM] head groups following the chlorides. Lesser solvent structuring was observed for the ringed compounds in [BMIM]Cl, with the most pronounced effects in the vicinity of the carbonyl group.

In addition, when present in larger concentrations, the different solutes show remarkably different propensities in their transport properties. The presence of carboxyl groups appears to both reduce the diffusivity of individual molecules as well as increase the likelihood of cluster formation, which will in turn lead to even lower diffusivities and greater viscosities. These trends, taken together, make the challenge of processing in ionic liquid solvents even more challenging.

Free energies of solvation were calculated for each solute and compared with simulation results. The formation of solute aggregates within the solvent could be quantified through the use of a dispersion measure, showing that generally the solutes remained well dispersed in each solvent. Moreover, solutes containing hydroxyl groups tended to show a certain uniformity in the solvent [BMIM]Cl.

Further investigation of dynamic dispersal of phase-separated solute droplets in [BMIM]Cl showed that hydroxyl ends present in a few of the solutes tended to complex with chloride ions. In the case of methylsuccinic acid, which has more strongly interacting carboxylate OH groups, chloride was found to bind ends of multiple solutes together, forming large chain-like complexes. This strong binding largely inhibits the dynamic dispersal of the solute throughout the solvent.

The results of this study suggest that careful attention needs to be paid to the solvation properties of derivatives obtained from cellulose in the design of cost-effective biorefinery processes. In particular, the interaction of strongly charged polar groups appears to greatly reduce the diffusivity and increase the tendency toward aggregation.

■ ASSOCIATED CONTENT

Supporting Information

Further details on the solvent structures used in the creation of the spatial distribution functions, information used in the diffusivity calculations, as well as further information concerning switching the Lennard-Jones parameters of MSA and MBD. This material is available free of charge via the Internet at http://pubs.acs.org.

■ AUTHOR INFORMATION

Corresponding Author

*E-mail: brooks.rabideau@avt.rwth-aachen.de.

Notes

The authors declare no competing financial interest.

■ ACKNOWLEDGMENTS

We thank Rolf Isele-Holder and Kai Leonhard for their helpful discussions and advice in using COSMO-RS. This work was performed as part of the Cluster of Excellence "Tailor-Made Fuels from Biomass", which is funded by the Excellence Initiative by the German federal and state governments to promote science and research at German universities.

■ REFERENCES

(1) Geilen, F. M. A.; Engendahl, B.; Harwardt, A.; Marquardt, W.; Klankermayer, J.; Leitner, W. *Angew. Chem.* **2010**, *49*, 5510.
(2) Youngs, T. G. A.; Hardacre, C.; Holbrey, J. D. *J. Phys. Chem. B* **2007**, *111*, 13765−13774.
(3) Chen, T.; Chidambaram, M.; Lin, Z.; SMIT, B.; Bell, A. T. *J. Phys. Chem. B* **2010**, *114*, 5790−5794.
(4) Engel, P.; Mladenov, R.; Wulfhorst, H.; Jaeger, G.; Spiess, A. C. *Green Chem.* **2010**, *12*, 1959−1966.
(5) Ignatyev, I. A.; Mertens, P. G. N.; Van Doorslaer, C.; Binnemans, K.; de Vos, D. E. *Green Chem.* **2010**, *12*, 1790−1795.
(6) Kahlen, J.; Masuch, K.; Leonhard, K. *Green Chem.* **2010**, *12*, 2172−2181.
(7) Liu, H.; Sale, K. L.; Holmes, B. M.; Simmons, B. A.; Singh, S. *J. Phys. Chem. B* **2010**, *114*, 4293−4301.
(8) Li, C.; Wang, Q.; Zhao, Z. K. *Green Chem.* **2008**, *10*, 177−182.
(9) Pinkert, A.; Marsh, K. N.; Pang, S.; Staiger, M. P. *Chem. Rev.* **2009**, *109*, 6712−6728.
(10) Gross, A. S.; Bell, A. T.; Chu, J.-W. *J. Phys. Chem. B* **2011**, *115*, 13433−13440.
(11) Hanke, C.; Atamas, N.; Lynden-Bell, R. *Green Chem.* **2002**, *4*, 107−111.
(12) Hanke, C.; Johansson, A.; Harper, J.; Lynden-Bell, R. *Chem. Phys. Lett.* **2003**, *374*, 85−90.
(13) Canongia Lopes, J. N.; Costa Gomes, M. F.; Padua, A. A. H. *J. Phys. Chem. B* **2006**, *110*, 16816−16818.
(14) Padua, A. A. H.; Costa Gomes, M. F.; Canongia Lopes, J. N. *Acc. Chem. Res.* **2007**, *40*, 1087−1096.
(15) Meng, E.; Kollman, P. *J. Phys. Chem.* **1996**, *100*, 11460−11470.
(16) Hernández-Cobos, J.; Ortega-Blake, I. *J. Chem. Phys.* **1995**, *103*, 9261−9273.
(17) Plimpton, S. *J. Comput. Phys.* **1995**, *117*, 1−19.
(18) Jorgensen, W.; Maxwell, D.; TiradoRives, J. *J. Am. Chem. Soc.* **1996**, *118*, 11225−11236.
(19) Berendsen, H. J. C.; Grigera, J. R.; Straatsma, T. P. *J. Phys. Chem.* **1987**, *91*, 6269−6271.
(20) Canongia Lopes, J. N.; Deschamps, J.; Padua, A. A. H. *J. Phys. Chem. B* **2004**, *108*, 2038−2047.
(21) Urahata, S.; Ribeiro, M. *J. Chem. Phys.* **2004**, *120*, 1855−1863.
(22) Cadena, C.; Zhao, Q.; Snurr, R.; Maginn, E. *J. Phys. Chem. B* **2006**, *110*, 2821−2832.
(23) Borodin, O. *J. Phys. Chem. B* **2009**, *113*, 11463−11478.
(24) Liu, Z.; Chen, T.; Bell, A.; Smit, B. *J. Phys. Chem. B* **2010**, *114*, 4572−4582.
(25) Chaban, V. V.; Voroshylova, I. V.; Kalugin, O. N. *Phys. Chem. Chem. Phys.* **2011**, *13*, 7910−7920.
(26) Sescousse, R.; Le, K.; Ries, M. E.; Budtova, T. *J. Phys. Chem. B* **2010**, *114*, 7222.
(27) Taguchi, R.; Machida, H.; Sato, Y.; Smith, R. L. *J. Chem. Eng. Data* **2009**, *54*, 22−27.
(28) Rafferty, J.; Maginn, E.; Siepmann, J. I. *Fluid Phase Equilib.* **2007**, *260*, 218−231.
(29) Shinoda, W.; Mikami, M. *J. Comput. Chem.* **2003**, *24*, 920−930.
(30) Hockney, R. W.; Eastwood, J. W. *Computer Simulation Using Particles*; Adam Hilger-IOP: Bristol, U.K., 1988.
(31) http://www.chemspider.com/.
(32) *CRC Handbook of Chemistry and Physics*, 89th ed. (Internet version 2009); Lide, D. R., Ed.; CRC Press/Taylor and Francis: Boca Raton, FL, 2009.
(33) Kirkwood, J. G.; Buff, F. P. *J. Chem. Phys.* **1949**, *17*, 338−343.
(34) Blokhuis, E.; Bedeaux, D.; Holcomb, C.; Zollweg, J. *Mol. Phys.* **1995**, *85*, 665−669.
(35) Chapela, G. A.; Saville, G.; Thompson, S.; Rowlinson, J. *J. Chem. Soc., Faraday Trans. 2* **1977**, *73*, 1133−1144.
(36) Sides, S. W.; Grest, S.; Gary; Lacasse, , M.-D. *Phys. Rev. E* **1999**, *60*, 6708.
(37) Ismail, A. E.; Grest, G. S.; Stevens, M. J. *J. Chem. Phys.* **2006**, *125*, 014702.
(38) Chowdhuri, S.; Chandra, A. *Phys. Rev. E* **2002**, *66*, 041203.
(39) Chandra, A. *Phys. Rev. Lett.* **2000**, *85*, 768−771.
(40) Luzar, A.; Chandler, D. *Phys. Rev. Lett.* **1996**, *76*, 928−931.
(41) Luzar, A. *J. Chem. Phys.* **2000**, *113*, 10663−10675.
(42) Luzar, A.; Chandler, D. *J. Chem. Phys.* **1993**, *98*, 8160−8173.
(43) Luzar, A.; Chandler, D. *Nature* **1996**, *379*, 55.

(44) Tsige, M.; Grest, G. S. *J. Am. Chem. Soc.* **2004**, *120*, 2989−2995.
(45) Mobley, D. L.; Dumont, E.; Chodera, J. D.; Dill, K. A. *J. Phys. Chem. B* **2007**, *111*, 2242−2254.
(46) Mobley, D. L.; Bayly, C. I.; Cooper, M. D.; Dill, K. A. *J. Phys. Chem. B* **2009**, *113*, 4533−45370.
(47) Mobley, D. L.; Bayly, C. I.; Cooper, M. D.; Shirts, M. R.; Dill, K. A. *J. Chem. Theory Comput.* **2009**, *5*, 350−358.
(48) Mobley, D. L.; Dumont, E.; Chodera, J. D.; Dill, K. A. *J. Phys. Chem. B* **2007**, *111*, 2242−2254.
(49) Paluch, A. S.; Mobley, D. L.; Maginn, E. J. *J. Chem. Theory Comput.* **2011**, *7*, 2910−2918.
(50) Shirts, M.; Pitera, J.; Swope, W.; Pande, V. *J. Chem. Phys.* **2003**, *119*, 5740−5761.
(51) Shirts, M.; Pande, V. *J. Chem. Phys.* **2005**, *122*, 134508.
(52) Klamt, A.; Eckert, F.; Arlt, W. *Annu. Rev. Chem. Biomol. Eng.* **2010**, *1*, 101−122.
(53) Klamt, A.; Diedenhofen, M. *J. Comput.-Aided Mol. Des.* **2010**, *24*, 357−360.
(54) Klamt, A.; Eckert, F. *COSMOtherm*, version C3.0, release 12.01; COSMOlogic GmbH and Co. KG: Leverkusen, Germany, 2012.
(55) Eckert, F.; Klamt, A. *AIChE J.* **2002**, *48*, 369−385.
(56) Clark, P.; Evans, F. *Ecology* **1954**, *35*, 445−453.